DOI 10.1007/s11094-018-1704-x
Pharmaceutical Chemistry Journal, Vol. 51, No. 10, January, 2018 (Russian Original Vol. 51, No. 10, October, 2017)

CAPTOPRIL-LOADED SUPERPARAMAGNETIC NANOPARTICLES AS A NEW DUAL-MODE CONTRAST AGENT FOR SIMULTANEOUS *IN VITRO/IN VIVO* MR IMAGING AND DRUG DELIVERY SYSTEM

Sajjad Abbasi Pour[1] and Hamid Reza Shaterian[1, *]

Original article submitted December 14, 2016.

Superparamagnetic iron oxide nanoparticles (SPIONs) are widely applied as magnetic resonance imaging (MRI) contrast agents and drug carriers in drug delivery systems (DDSs) for diagnostics and treatment of diseases. Observation of drug delivery, drug release, and monitoring of the treatment can be performed by MRI. Magnetic nanoparticles (MNPs) can be used as dual-mode agents for simultaneous MRI contrast and drug delivery. Application of dual-mode MRI-contrast and drug-carrier agent is especially useful in targeted DDS. In this study, we report on the preparation of captopril-coated MNPs as a new dual-mode agent for simultaneous MRI contrast and DDS. The influence of contrast agent on the longitudinal (*T1*) and transverse (*T2, T2**) relaxation times was studied and it was found that the effect on *T2* and *T2** exceeds the effect on *T1*, which leads to darkening of the MR image. Release of captopril from γ-Fe_2O_3@SiO_2@captopril system was studied at three pH values and it was established that the drug release at pH 1.2 was greater than that at pH 4.8 and 7.4. The obtained results show that MNPs loaded with captopril can be used as dual-mode MRI contrast agent and DDS system.

Keywords: captopril-loaded magnetic nanoparticles; dual-mode agent, MRI contrast agent; drug delivery system.

1. INTRODUCTION

Angiotensin-converting enzyme (ACE) inhibitors have been conclusively shown to improve long-term prognosis in human heart failure trials [1, 2]. ACEs play an important role in the control of arterial blood pressure. ACE catalyzes the conversion of decapeptide (angiotensin I) to the potent vasoconstring octapeptide (angiotensin II). Inhibition of ACE activity leads to decrease in the concentration of angiotensin II and consequently reduces blood pressure [3, 4]. Several ACE inhibitors, for example captopril, enalapril, and lisinopril are in clinical use for treatment of hypertension [5]. Captopril inhibits conversion of the relatively inactive angiotensin I to the angiotensin II according to the mechanism proposed by Ondetti and colleagues [6]. Captopril, which is water soluble, is usually prescribed to patients who are chronically ill and require long-term use for its therapeutic benefits. It is regarded as a preferred drug in antihypertensive therapy because of its effectiveness, low price, and low toxicity. It is a first-line drug for treatment of various types of hypertension, congestive heart failure, kidney problems caused by diabetes, and to improve survival after a heart attack [7].

In the past few years, drug delivery systems (DDSs) have attracted a great deal of attention in order to improve therapeutic efficacy and overcome side effects [8]. SPIONs such as magnetite (Fe_3O_4) and its oxidized form maghemite (γ-Fe_2O_3) have widespread applications in magnetic bioseparation, drug delivery, magnetic resonance imaging, magnetic-field-assisted radionuclide therapy and especially in targeted drugs. One of the most promising targeting methods is using magnetic particles loaded with drugs due to their excellent magnetic properties together with low toxicity and biocompatibility [9 – 13]. Nanoporous silica-based materials have attracted much attention for their potential applications in drug delivery due to their excellent biocompatibility, very high surface areas available for the loading of drug molecules, and diversity in surface functionalization [14].

To improve the signal-to-noise ratio (SNR) of images and create high-quality anatomical images of the body, including deep tissues, organs and tumors for early diagnosis and treatment monitoring, superparamagnetic iron oxide nanoparticles (SPIONs) as contrast agents are usually neces-

[1] Department of Chemistry, Faculty of Sciences, University of Sistan and Baluchestan, PO Box, 98135-674, Zahedan, Iran.
[*] e-mail: hrshaterian@chem.usb.ac.ir

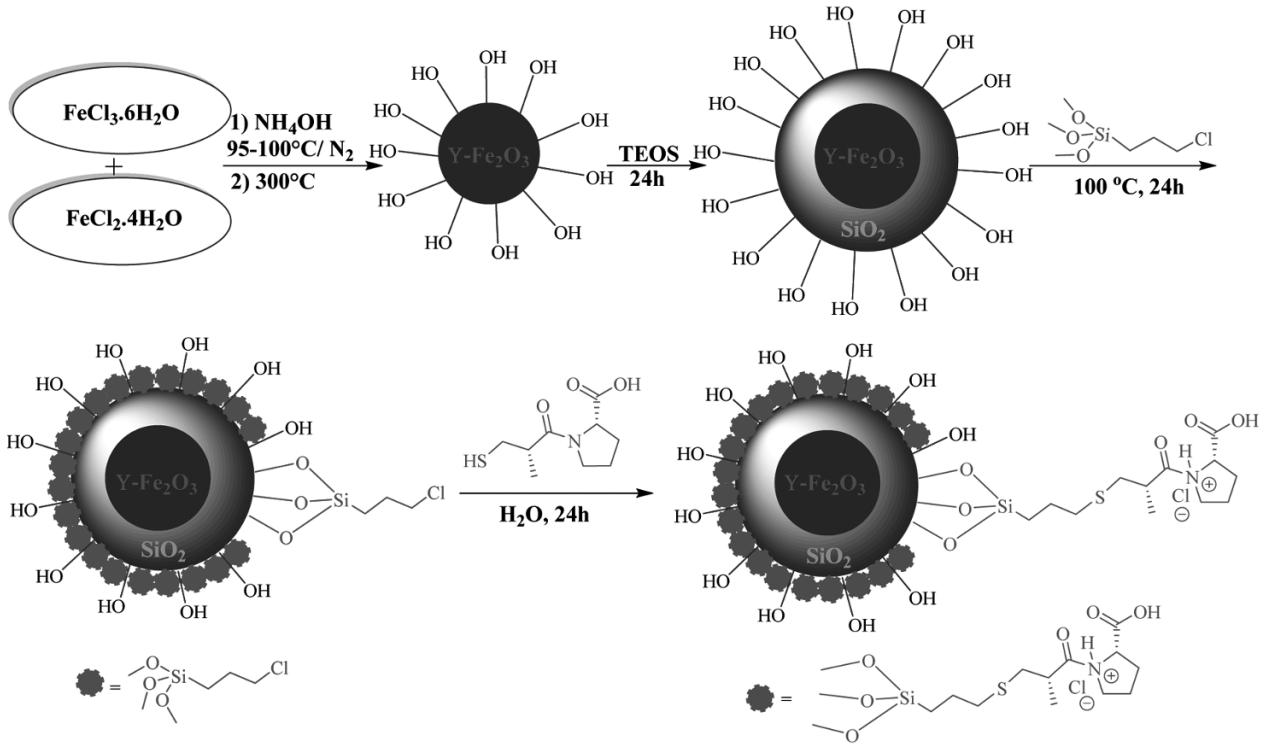

Fig. 1. Schematic representation of the synthesis, modification of SPIONs with SiO_2, and captopril loading to yield the dual-mode contrast agent for simultaneous MRI and DDS.

sary for magnetic resonance imaging (MRI) [15, 16]. For example, SPIONs can shorten the *T2* and *T2** values of a tissue and thus provide a negatively enhanced contrast signal for MRI techniques [17]. Advantages of *T2* negative contrast agents are low toxicity, large r_2/r_1 ratio, and good biocompatibility, and they can be detected at smaller concentrations in clinical use [18]. When the drug is loaded into a nanocarrier for targeted DDS, observation of drug delivery, drug release, and monitoring of the treatment can be performed by available imaging modalities such as MRI, computed tomography, near-infrared fluorescence imaging, ultrasonic and photoacoustic methods [19]. The large surface-to-volume ratio of NPs can be modified with biologically compatible molecules and drugs, which allows for simultaneous diagnostics and therapy [20].

In this work, we report captopril-coated MNPs as a new dual-mode contrast agent for simultaneous MRI and DDS. For this purpose, we first synthesized captopril-coated MNPs and then characterized it with various techniques. The impact of contrast agent on the longitudinal (*T1*), and transverse (*T2*, *T2**) relaxation times was tested and it was determined that the effect of contrast agent on *T2*, *T2** relaxation times is greater than on *T1* value and leads to darkening of the MR image. Also we tested the drug release from captopril-coated MNPs at three (1.2, 4.8, and 7.4) pH values.

2. RESULTS AND DISCUSSION

2.1. Chemicals

Captopril ($C_9H_{15}NO_3S$, >98%, Sigma–Aldrich) was a gift from Tehran Daroo Pharmaceutical Company (Iran). Ferrous chloride tetrahydrate ($FeCl_2{\cdot}4H_2O$, 99%), ferric chloride hexahydrate ($FeCl_3{\cdot}6H_2O$, 99%), tetramethylammonium ($C_4H_{13}ON$, 97%), tetraethyl orthosilicate ($C_8H_{20}O_4Si$, 99%), and (3-chloropropyl)trimethoxysilane ($C_6H_{15}O_3SiCl$, >97%) were obtained from Sigma–Aldrich. Absolute ethanol (C_2H_5OH, >99.9%) and NH_4OH were supplied from Merck company. All the materials were used without any purification. Fe_3O_4 nanoparticles were synthesized by a reported chemical co-precipitation technique from ferric and ferrous ions in ammonia solution with minor modifications [21 – 24].

2.2. Synthesis

Synthesis of γ-Fe_2O_3 nanoparticles. First, $FeCl_2 \cdot 4H_2O$ (0.802 g) and $FeCl_3{\cdot}6H_2O$ (2.184 g) were dissolved in water (10 mL) separately and then mixed in a 500 mL three-neck flask at room temperature. Then, NH_4OH solution (0.7 M, 100 mL) was added dropwise in 5 – 10 min to the mixture stirring on magnetic mixer (TWCLL-T, DF-101S) at room temperature to adjust the reaction at pH 11. The precipitate

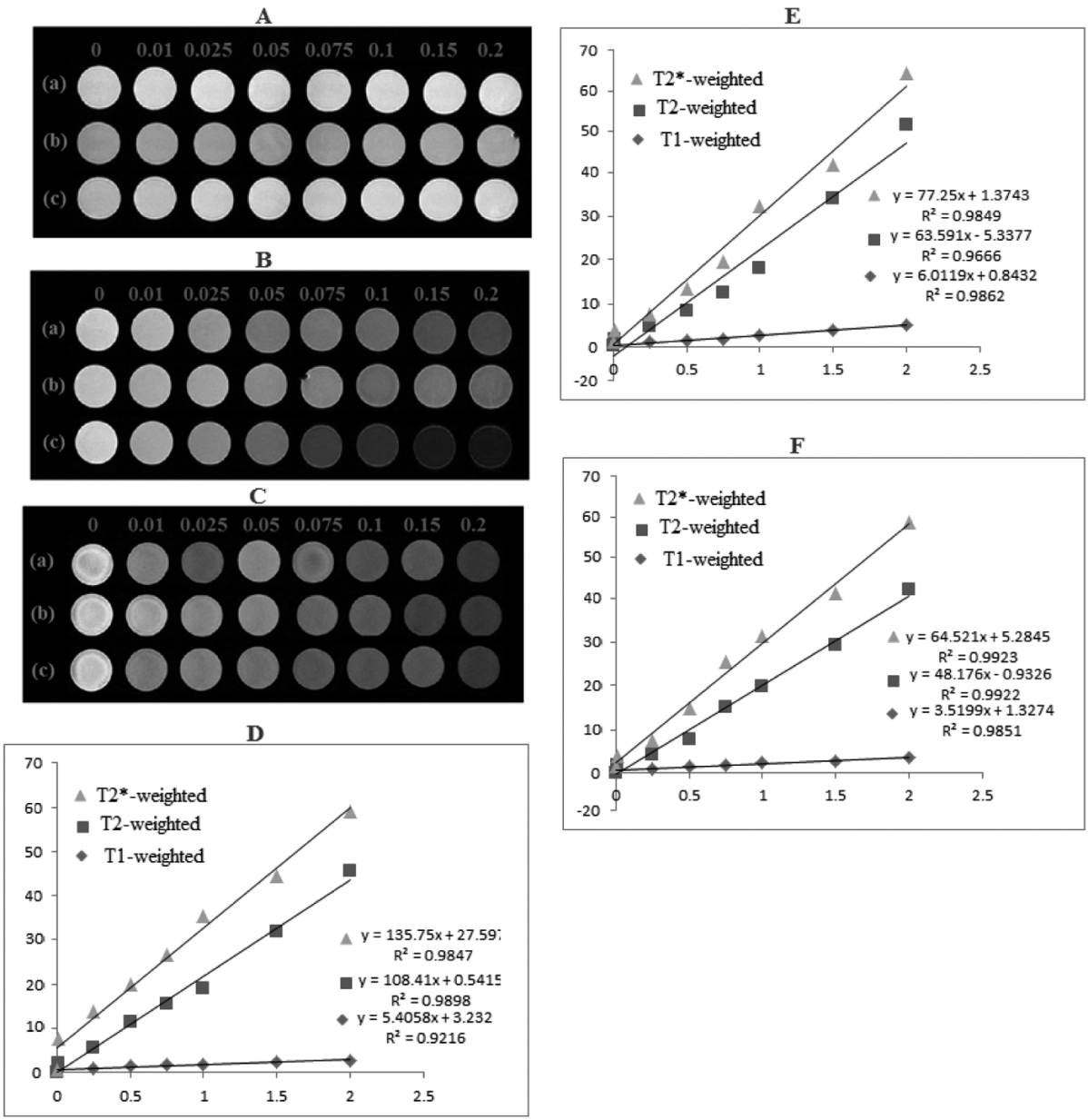

Fig. 2. (A) T1-weighted, (B) *T2*-weighted and (C) *T2**-weighted images of (a) γ-Fe_2O_3, (b) γ-Fe_2O_3@SiO_2 and (c) γ-Fe_2O_3@SiO_2@captopril, respectively; (D) plots of longitudinal relaxivity *R1, R2* and *R2**for γ-Fe_2O_3@SiO_2@captopril; (E) plots of longitudinal relaxivity *R1, R2* and *R2**for γ-Fe_2O_3@SiO_2;; (F) plots of longitudinal relaxivity *R1, R2* and *R2**for γ-Fe_2O_3.

was separated with strong external magnet, decantated, and washed three times with deionized water to remove any ions. Then, solution of tetramethylammonium hydroxide (1 – 2 mL) was added dropwise to the magnetic nanoparticles, quickly stirred, and separated with external magnet. The dried precipitate of Fe_3O_4 kept in the furnace for 3 h at 300°C to give a reddish-brown powder of γ-Fe_2O_3 nanoparticles.

Synthesis of γ-Fe_2O_3@SiO_2 nanoparticles. A mixture of γ-Fe_2O_3 (2 g) in ethanol (40 mL) was sonicated for 30 min in an ultrasonic bath (frequency, 40 kHz; power, 40 kW) and then heated for 1 h at 40 °C. Subsequently, tetraethyl orthosilicate (TEOS, 10 mL) was added to the reaction vessel, and the mixture was continuously stirred for 24 h. The silica-coated nanoparticles were collected by external magnet, washed three times with EtOH and diethyl ether, and dried at 100 °C in vacuum for 12 h.

Synthesis of chloro-functionalized γ-Fe_2O_3@SiO_2 nanoparticles. A mixture of γ-Fe_2O_3@SiO_2 (2 g) in dry toluene (40 mL) was sonicated for 45 min. Then, 3-chloropropyl trimethoxysilane (1 mL) was added to the dispersed

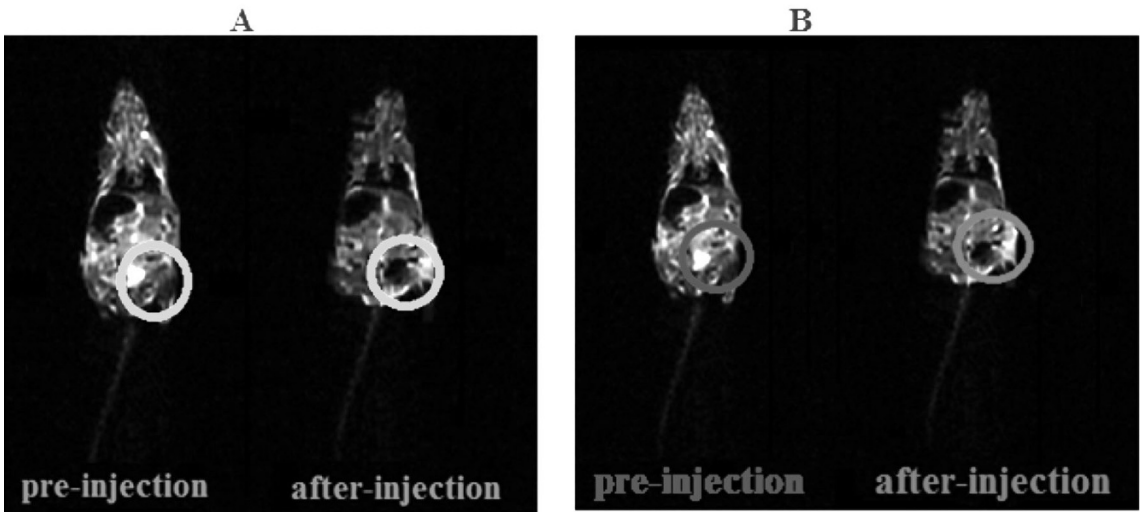

Fig. 3. *T2*-weighted (A) and *T2**-weighted (B) MRI images of mice recorded pre- and after-injection of MNPs with captopril.

γ-Fe_2O_3@SiO_2 in toluene and slowly heated to 100 °C. The reaction mixture was stirred at this temperature for 24 h. The precipitate was separated by external magnet, washed three times with EtOH and diethyl ether, and then dried at 12 h at 40 °C in an oven.

Synthesis of γ-Fe_2O_3@SiO_2@captopril nanoparticles. Solution of chloro-functionalized γ-Fe_2O_3@SiO_2 (1 g) in deionized water (15 mL) in a 50 mL round-bottom flask was sonicated for 30 min and then was added captopril (0.3 g) dissolved in 10 mL of H_2O. Then, the reaction mixture was stirred at RT overnight with a magnetic stirring bar. The precipitate was separated by external magnet, washed three times with EtOH and diethyl ether, and dried for 12 h at 40 °C in an oven.

Thus, the desired dual-mode contrast agent for simultaneous MRI and DDS was formed as illustrated in Fig. 1.

2.3. Characterization Techniques

The obtained contrast agent was characterized by various techniques including SEM, EDS, TGA, XRD, VSM, and FT-IR spectroscopy.

FT-IR spectra of nanoparticles were taken with a Bruker a JASCO FT-IR460 Plus spectrophotometer in the range of 400 – 4000 cm^{-1} as KBr disks. The elemental composition was determined with a Leo 1450 VP scanning electron microscope equipped with an SC7620 energy dispersive spectrometer (SEM-EDS) presenting a 133 eV resolution at 20 kV. The particle size distribution of the prepared contrast agent was determined by dynamic light scattering (DLS) (Malvern Instruments, UK, model Nano ZS). The structure and crystal phase of the contrast agent were determined by a Bruker D8 x-ray diffractometer with Cu*K*α radiation (λ = 1.54 Å) operated at 40 kV and 30 mA.

The morphology and particle size of γ-Fe_2O_3@SiO_2@captopril contrast agent was demonstrated using the scanning electron microscopy (SEM). The SEM image (Fig. 6) represents shape and spherical morphology of nanoparticles and also shows their average size 26.4 nm. The sizes of nanoparticles were analyzed by DLS technique. According to the particle size distribution curve, the average size of nanoparticles was specified to be 15.6 nm, which is smaller than the size of particles according to SEM because the SEM measurement is performed under dry conditions.

The composition of the γ-Fe_2O_3@SiO_2@captopril particles was analyzed using energy dispersive x-ray spectroscopy (EDS). The EDS results (Fig. 7) clearly show the presence of Fe, O, Si, S, C, N, and Cl atoms in the contrast agent and indicate that magnetic nanoparticles are functionalized by captopril compound. According to the EDS analysis, it can be deduced that desired γ-Fe_2O_3@SiO_2@captopril particles have been successfully synthesized.

TABLE 1. Parameters r_1, r_2 and r_2* of γ-Fe_2O_3, γ-Fe_2O_3@SiO_2, and γ-Fe_2O_3@SiO_2@captopril MNPs

Nanoparticles	r_1 ($mM^{-1}s^{-1}$)	r_2 ($mM^{-1}s^{-1}$)	r_2* ($mM^{-1}s^{-1}$)	r_2/r_1 ($mM^{-1}s^{-1}$)	r_2*/r_1 ($mM^{-1}s^{-1}$)
γ-Fe_2O_3	3.5199	48.176	64.521	13.686	18.33
γ-Fe_2O_3@SiO_2	6.0119	63.591	77.25	10.577	12.849
γ-Fe_2O_3@SiO_2@captopril	5.4058	108.41	135.75	20.054	25.111

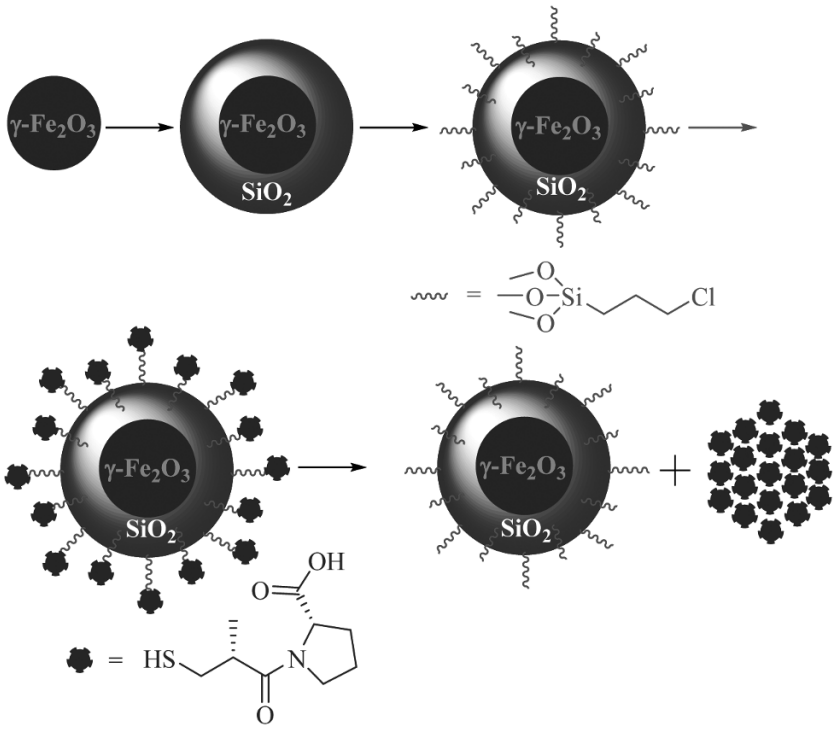

Fig. 4. Schematic representation of the preparation and drug release from γ-Fe_2O_3@SiO_2@captopril MNPs.

The x-ray powder diffraction (XRD) was applied to specify the crystalline structure of γ-Fe_2O_3@SiO_2@captopril (Fig. 8). On the basis of XRD data, the synthesized magnetic nanoparticles (γ-Fe_2O_3@SiO_2@captopril), represent diffraction peaks at 2θ 30.3, 35.7, 43.4, 53.8, 74.5, and 62.9° corresponding to the (220), (311), (400), (422), (511) and (440) reflections of γ-Fe_2O_3 and demonstrating the structure of MNPs. The XRD pattern of γ-Fe_2O_3@SiO_2@captopril showed that SiO_2 and captopril formed an amorphous phase and only γ-Fe_2O_3 nanoparticles were crystalline (JCPDS file No 04-0755).

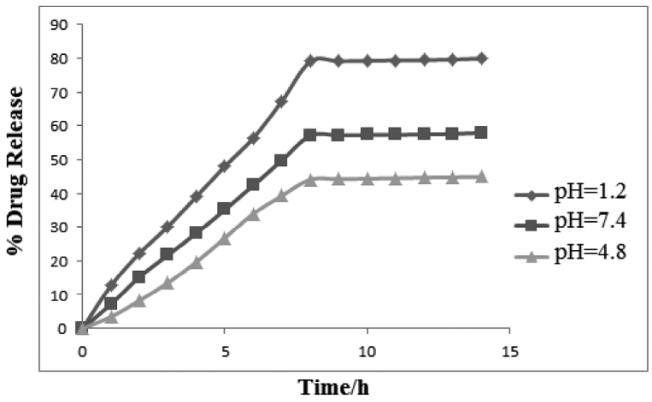

Fig. 5. Profiles of captopril release from γ-Fe_2O_3/SiO_2/captopril MNPs at pH 7.4, 5.8, and 1.2 at 37 ^oC.

To evaluate the magnetic properties of MNPs with captopril, the vibrating sample magnetometry (VSM) was used in an applied field of approximately 10000 Oe at room temperature. The VSM graphs of MNPs and MNPs with captopril are displayed in Fig. 9**.** Clearly, both MNPs and MNPs with captopril show superparamagnetic behavior. As it can be observed, the saturation magnetization (MS) value of MNPs is approximately 59 emu/g. The saturation magnetization of γ-Fe_2O_3@SiO_2@captopril contrast agent in comparison to the uncoated γ-Fe_2O_3 MNPs (68 emu/g) exhibited evident decrease because of the increased amount of organic compound on the nanoparticle surface. The strong magnetization of the MNPs was specified by means of an external magnet (Fig. 9, right inset) indicating that the synthesized magnetic nanoparticles had superb magnetic responsivity, which enables them to be easily driven by external magnetic field.

The FT-IR spectra of γ-Fe_2O_3, γ-Fe_2O_3@SiO_2@captopril and captopril in the wavenumber range 4000 – 400 cm^{-1} are depicted in Fig. 10**.** As can be seen, FT-IR spectra clearly confirm the synthesis of contrast agent**.** In the FT-IR spectrum of captopril (Fig. 10a), the broad peak in 2400 – 3600 cm^{-1} is related to O-H of carboxylic acid functional group of captopril; the peak at 2980 cm^{-1} is due to the C-H group; the particular band at 1748 cm^{-1} is attributed to stretching vibration of C=O carbonyl functional group; ab-

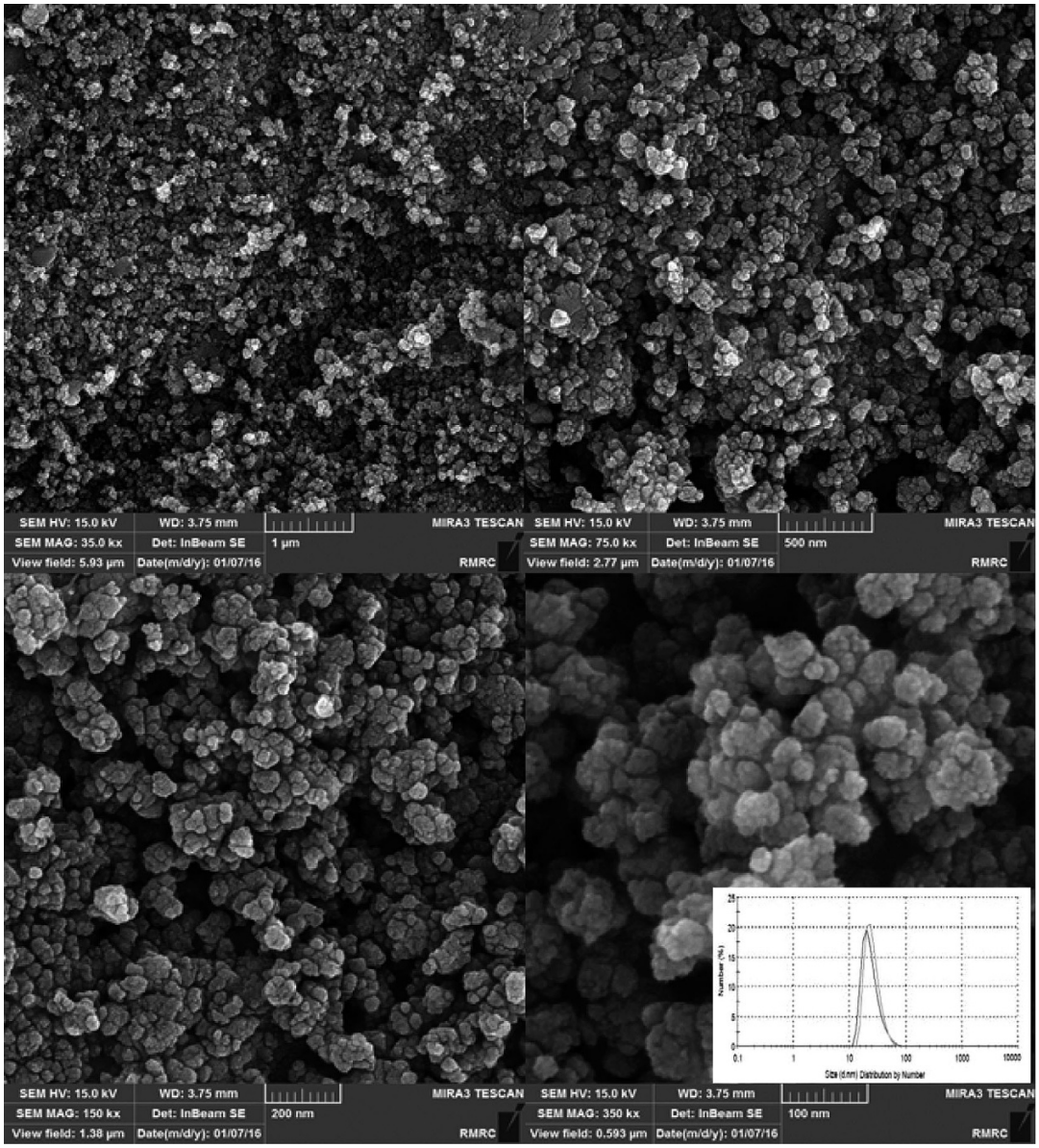

Fig. 6. SEM image and size distribution histogram of MNPs with captopril.

sorption bands of C-O and C-N functional groups can be seen in the region of 1100 – 1350 cm^{-1}. As shown in Fig. 10b, the FT-IR spectrum of γ-Fe_2O_3 nanoparticles represents particular IR absorption band in the region of 450 – 550 cm^{-1}, which is ascribed to the stretching vibration of the Fe-O band and wide peak in 3100 – 3600 cm^{-1} can be attributed to O-H stretching vibration of hydroxyl functional groups of MNPs. FT-IR analysis (Fig. 10c) was accomplished to characterize the presence of the captopril compound on the MNPs. The FT-IR spectrum of γ-Fe_2O_3@SiO_2@captopril (Fig. 10c) is clearly different from those of γ-Fe_2O_3 (Fig. 10b) and captopril (Fig. 10a). The stretching mode of Si–O-Si showed a strong broad peak at about 1099 – 1220 cm^{-1}, while a strong broad peak at about 3600 – 2400 cm^{-1} is attributed to carboxylic acid functional group. The particular bands at 1621 cm^{-1} and 1937 cm^{-1} are attributed to the C=O and C-H functional groups, respectively.

Thermal gravimetric analysis (TGA) was studied to assess the stability of γ-Fe_2O_3@SiO_2@captopril particles (Fig. 11)**.** As can be seen from the TGA curve, the contrast agent demonstrated two mass loss steps. At the first step, a small weight loss below 200 °C is due to solvent desorption. The second weight loss at 200 – 500 °C can be attributed to the decomposition of the immobilized organic part. The total weight loss was computed to be 8% and the amount of captopril loaded on γ-Fe_2O_3@SiO_2 amounted to 0.37 mmol/g.

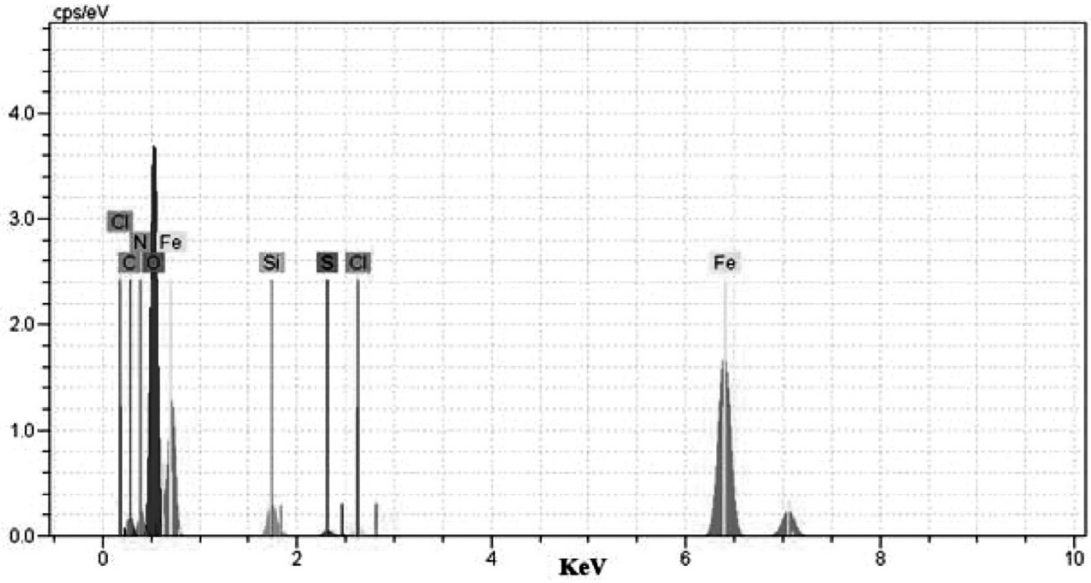

Fig. 7. EDS spectrum of MNPs with captopril.

The particle size distribution and zeta potential of the MNPs with captopril were determined by dynamic light scattering (DLS) spectrometry in aqueous solution. The value of the zeta potential is predictive of the colloidal stability. Nanoparticles with zeta potential values greater than +25 mV or less than -25 mV typically have high degrees of stability [26]. The zeta potential of γ-Fe_2O_3@SiO_2@captopril in aqueous dispersion (Fig. 12) was determined to be –28.2 mV that demonstrated high stability of MNPs with captopril.

The synthesis of γ-Fe_2O_3@SiO_2@captopril nanoparticles was also studied by ultraviolet-visible (UV-Vis) absorption spectroscopy. The absorption spectrum of aqueous solutions of γ-Fe_2O_3, captopril, and γ-Fe_2O_3@SiO_2@captopril is shown in Fig. 13. It demonstrates that γ-Fe_2O_3@SiO_2@captopril in comparison to pure captopril has a decreased absorption band at 203 nm. This absorption band confirms successful synthesis of γ-Fe_2O_3@SiO_2@captopril nanoparticles.

2.4. Magnetic Resonance Imaging (MRI) Contrast Measurements

For assessing the magnetic relaxation properties of the contrast agent, MR images of γ-Fe_2O_3, γ-Fe_2O_3@SiO_2 and

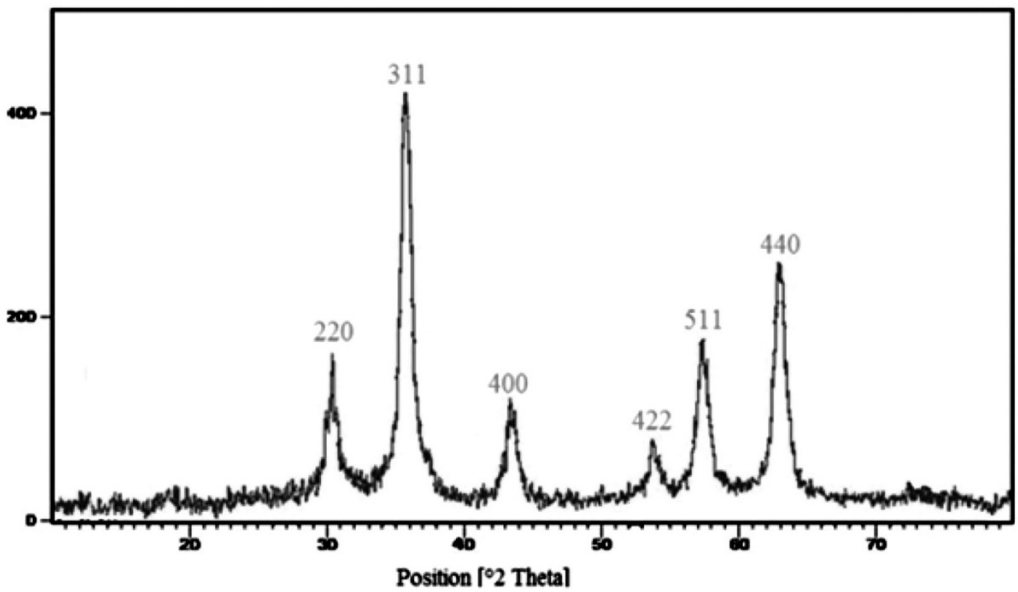

Fig. 8. XRD pattern of γ-Fe_2O_3@SiO_2@captopril MNPs.

γ-Fe_2O_3@SiO_2@captopril solutions with various iron concentrations (0, 10, 25, 50, 75, 100 , 150 and 200 μM) were measured by using a clinical 1.5 T whole body MR scanner (Siemens Healthcare Avanto Germany) at 25 °C. *T1*-weighted images were measured by applying the spin echo imaging sequence at various repetition times (100, 1550, 3150, 4750 and 6400 ms) with an echo time of 18 ms; slice thickness, 7.5 mm; field of view (FOV), 230; and matrix, 200 × 256. The *T2*-weighted images were obtained by using in the spin echo sequence with repetition times (*TR*) of 1600 ms and varying echo time (*TE*) of 10, 43, 75, 108 and 140 ms; slice thickness, 7.5 mm; field of view (FOV), 238; turbo factor, 18; matrix, 176 × 384. The *T2**-weighted images were measured with applying FOV = 240 mm^2; slice thickness, 4 mm; *TE* = 15 ms; *TR* = 350 ms; matrix, 288 × 160. The mean signal intensity of MRI images with different concentrations of magnetic nanoparticle were determined using of the Dicom Works 1.3.5 software and the region-of-interest (ROI) analysis was performed to distinguish signal intensities of each sample and assess the *R1, R2* and *R2** values. Relaxivities (r_1, r_2 and r_2*) were generally defined as the slope of the linear regression generated from plots of the measured relaxation rates (1/*T1*, 1/*T2*, and 1/*T2**) versus the concentration of MNPs [27 – 30].

$$SI = P_0\left[1-\exp\left(-\frac{TR}{T1}\right)\right], \quad (1)$$

$$SI = P_0\left[1-\exp\left(-\frac{TE}{T2}\right)\right], \quad (2)$$

$$SI = P_0\left[1-\exp\left(-\frac{TE}{T2*}\right)\right], \quad (3)$$

where *SI* is the signal intensity and P_0 is constant factor. The longitudinal relaxivity r_1, transverse relaxivity r_2, and transverse relaxivity r_2*, which characterize the performance of captopril-coated MNPs as contrast agents, were calculated from the slopes of linear relationships (1) – (3) [31, 32].

MRI contrast enhancement (*in vitro* image). The longitudinal (*T1*), transverse (*T2*) and transverse (*T2**) relaxation times were measured at various solutions of different nanoparticles concentration using a clinical 1.5 T whole body MR scanner. In general, longitudinal relaxivity (r_1), transverse relaxivity (r_2) and transverse relaxivity (r_2*) are used to evaluate the ability to alter spin-lattice relaxation (*T*1), spin-spin relaxation (*T2*) and spin-spin relaxation (*T2**) in the MRI, respectively [33]. To prove that γ-Fe_2O_3@ SiO_2@ captopril is good MRI contrast agent, we applied γ-Fe_2O_3 and γ-Fe_2O_3@SiO_2 as contrast agents in comparison to γ-Fe_2O_3@SiO_2@captopril. Figures 2A, 2B, and 2C show *T1*-, *T2*- and *T2**-weighted MR images of γ-Fe_2O_3, γ-Fe_2O_3@SiO_2, and γ-Fe_2O_3@SiO_2@captopril, respectively, with iron concentrations 0, 10, 25, 50, 75, 100, 150 and 200 μM in deionized water. These MRI data show that growing MNPs concentration leads to increase in the signal intensity of *T1*-weighted images whereas the signal intensity of *T2*- and *T2**-weighted images decreases. When water molecules are absorbed on the surface of magnetic nanoparticles by electrostatic attraction, then protons of the absorbed water molecules are easily influenced by the dipole moment of magnetic nanoparticles [29, 34 – 36]. Hence, the signal intensity of *T2*- and *T2**-weighted images is reduced and, as a result, the contrast of *T2*- and *T2**-weighted images is improved. The r_1, r_2 and r_2* values of γ-Fe_2O_3, γ-Fe_2O_3@SiO_2, and γ-Fe_2O_3@SiO_2@captopril were calculated from the slopes of 1/*T*1 (R_1), 1/*T2* (R_2) and 1/*T2** (R_2*) plots versus Fe concentration, showing that the relaxation rates linearly increase with the concentration (see Figs. 2D, 2E), and 2F). The calculated r_1, r_2, r_2* and r_2/r_1, r_2*/r_1 values of γ-Fe_2O_3, γ-Fe_2O_3@SiO_2, and γ-Fe_2O_3@SiO_2@captopril are shown in Table 1**.** The r_2/r_1 and r_2*/r_1 ratios demonstrate that γ-Fe_2O_3@SiO_2@captopril MNPs provide a much better contrast than γ-Fe_2O_3 and γ-Fe_2O_3@SiO_2 nanoparticles. The MR images showed that MNPs with captopril can significantly decrease the *T2* and *T2** relaxivity values and enhance the negative contrast signal of MRI, which makes the images darker than in the case without the MRI contrast agent. The r_2 and r_2* values show a strong dependence on the MNPs concentration. There is a significant difference in average transverse relaxivities between superparamagnetic γ-Fe_2O_3 (r_2= 48.176 and r_2*= 64.521 $mM^{-1}s^{-1}$), γ-Fe_2O_3@SiO_2 (r_2= 63.591 and r_2*= 77.25 $mM^{-1}s^{-1}$) and γ-Fe_2O_3@SiO_2@ captopril (r_2= 108.41 and r_2*= 135.75 $mM^{-1}s^{-1}$). The contrast of *T2*- and *T2**-weighted MR images obtained using MNPs with captopril is noticeably higher than that of clinically used iron oxide-based *T2*-type contrast agents. The MNPs with captopril effectively enhance *T2* and *T2**-contrast at 1.5 T, showing better performance than commercial alternatives [37]. Thus, the *in vitro* MR imaging results indi-

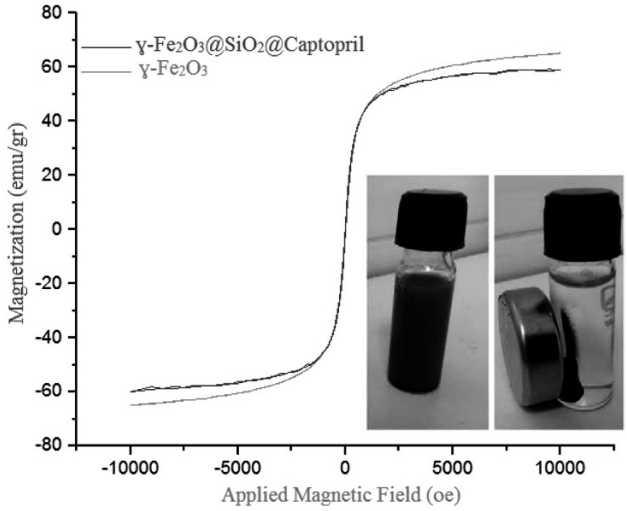

Fig. 9. VSM diagrams of γ-Fe_2O_3 and γ-Fe_2O_3@SiO_2@captopril MNPs.

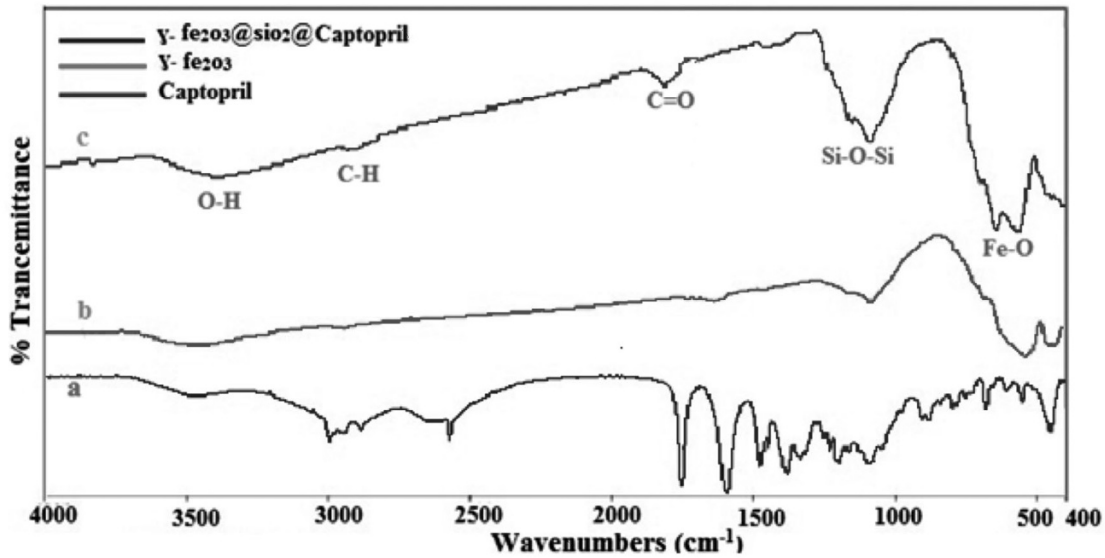

Fig. 10. FT-IR spectra: (a) captopril; (b) γ-Fe_2O_3; (c) γ-Fe_2O_3@SiO_2@captopril MNPs.

cate the ability of MNPs with captopril to be used as a contrast agent in the *T2*- and *T2**-weighted MRI.

In vivo* responsive *T2* and *T2* imaging. To demonstrate the potential of γ-Fe_2O_3@SiO_2@captopril nanoparticles as negative contrast agent we prepared *in vivo* MR images of mouse before and after injection of MNPs with captopril. *T2* and *T2**-weighted MR imaging with γ-Fe_2O_3@SiO_2@captopril was performed on mice bearing 4T1 tumor. The same conditions such as instrument and protocols were used for *in vivo* and *in vitro* MR imaging. The 4T1 cell line and 8-week-old female BALB/c mice (body weight, ~35_g) were obtained from the Pasteur Institute of Iran (Tehran, Iran). To obtain 4T1 murine breast tumor model, 5×10^6 4T1 cells suspended in PBS (100 μL) were

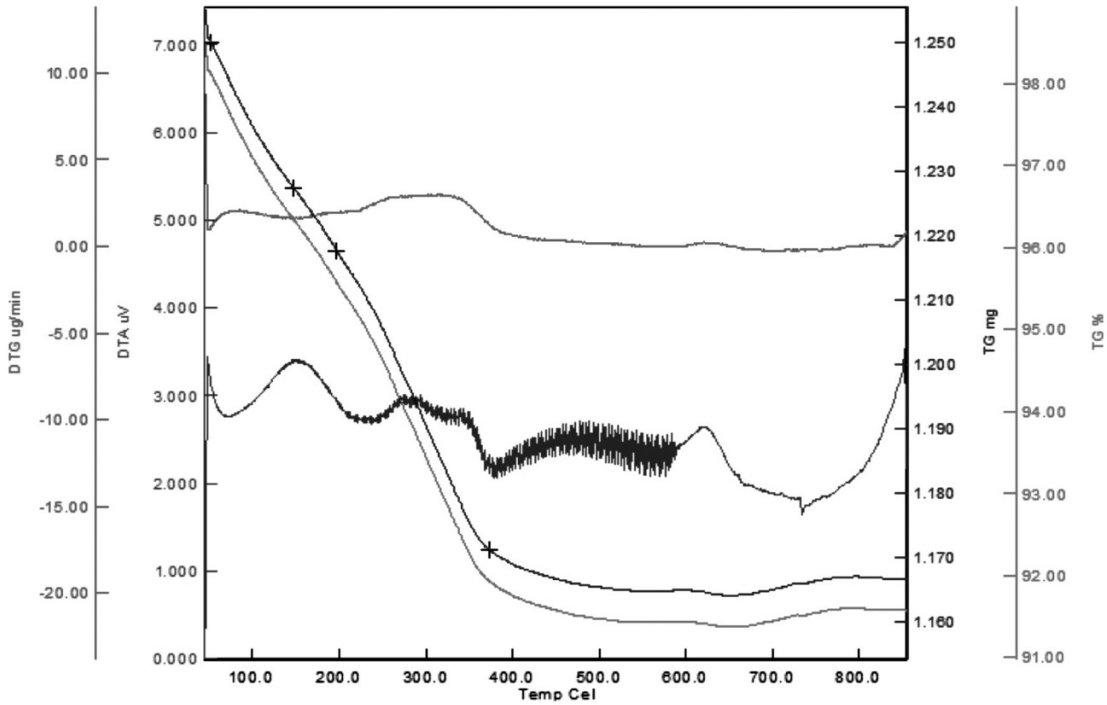

Fig. 11. TGA and DTG curves of MNPs with captopril.

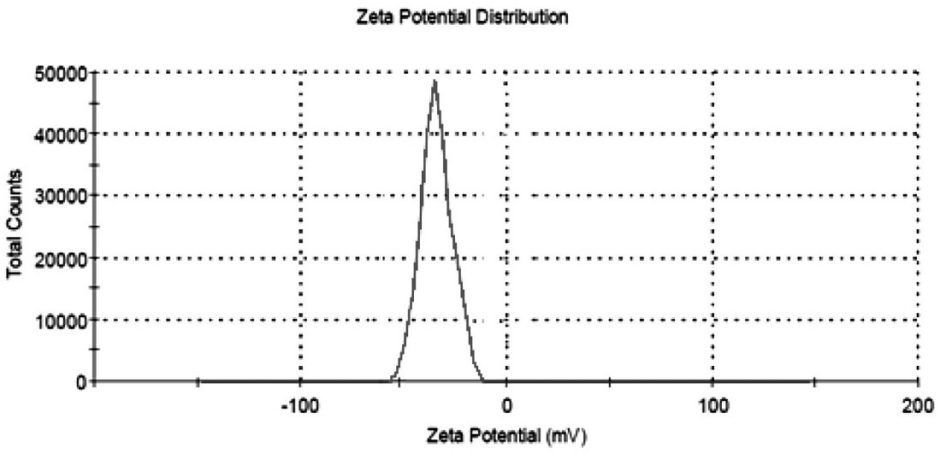

Fig. 12. Zeta potential of MNPs with captopril.

subcutaneously injected into the mice. During implantation, the mice were anesthetized with the mixture of ketamin (10%) and xylazine (2%) by intramuscular injection [30]. The MRI was carried out on these mice in 15 days, after which the tumor was established [38]. The *T2*- and *T2**-weighted images of mice were recorded for 200 μM concentration of MNPs with captopril before and 30_min after subcutaneous injection. As shown in Fig. 3, both the *T2*- and *T2**-weighted MR images were recorded before subcutaneous injection of γ-Fe_2O_3@SiO_2@captopril and 30 min after the subcutaneous injection. A darkened signal from the tumor can be detected in the *T2*- and *T2**-weighted images in MR imaging after the injection γ-Fe_2O_3@SiO_2@ captopril in comparison to the pre-injection image. As a result, a negative contrast agent for *T2*- and *T2**-weighted MRI could be well observed after subcutaneous injection of a suspension of MNPs with captopril into mice with 4T1 breast tumor. Thus, *in vivo* MRI results show the potential of γ-Fe_2O_3@SiO_2@captopril for clinical applications.

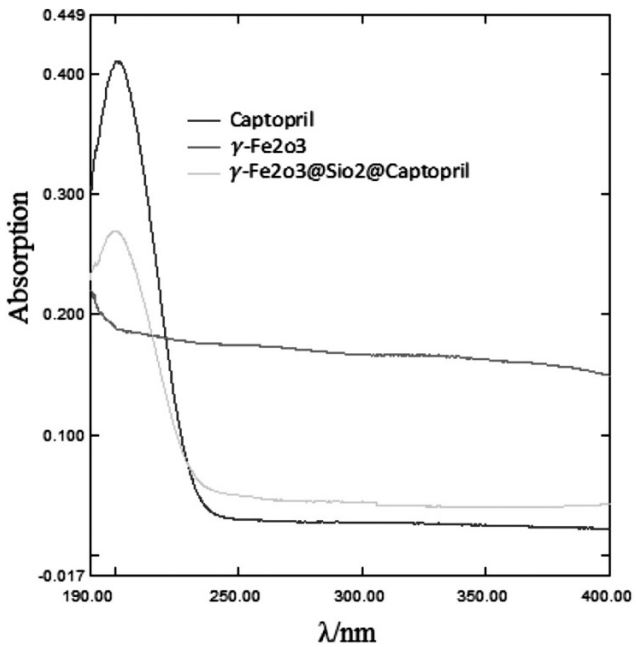

Fig. 13. UV-Vis absorption spectra of γ-Fe_2O_3, captopril, and γ-Fe_2O_3@SiO_2@captopril MNPs.

2.5. Captopril Loading and Release from γ-Fe_2O_3@SiO_2@*captopril MNPs*

The percentage of captopril loaded on MNPs was determined using the TGA (Fig. 11) and UV-Vis spectroscopy measurements. The obtained TGA results show that the maximum amount of captopril loaded on γ-Fe_2O_3@SiO_2 is 8% and in 100% γ-Fe_2O_3@SiO_2@captopril is equivalent to 0.37 mmol/g. The UV-Vis absorption spectroscopy data (Fig. 13) confirm the results obtained by TGA.

Figure 4 shows a schematic representation of the preparation of γ-Fe_2O_3@SiO_2@captopril and a diagram of captopril release from γ-Fe_2O_3@SiO_2@captopril MNPs. The *in vitro* drug release investigations of captopril-coated MNPs were carried out by paddle method in USP dissolution apparatus (Dissolution Tester DR-1, 230V AV/50 HZ/2 Amp). The MNPs with captopril is a pH-sensitive DDS that releases different amounts of drug from γ-Fe_2O_3@SiO_2@captopril at various pH. Samples of specified amounts of MNPs with captopril were placed into the USP dissolution apparatus. First, 100 mg of MNPs with captopril was dispersed in 900 mL buffer solution. The sample was charged into the dissolution apparatus, the power turned on, and the temperature and the rotating speed of the apparatus were adjusted at 37 °C and 55 rpm, respectively. At specified time intervals, 10 mL of sample was withdrawn and then replaced with 10 mL of fresh buffer. In order to measure the concentration of captopril released from γ-Fe_2O_3@SiO_2@captopril MNPs, UV-Vis spectrophotometer was used at λ_{max} = 203 nm. The

drug release investigations were carried out until no more change was observed in the absorbance of the medium. This procedure was used in order to estimate captopril release profile at three pH adjusted using 0.1N hydrochloric acid (pH 1.2), acetate buffer (pH 4.8), and phosphate buffer (pH 7.4). Figure 5 shows the profiles of captopril release from the γ-Fe_2O_3@SiO_2@captopril nanoparticles in pH, 0.1N hydrochloric acid (pH 1.2), acetate buffer (pH 4.8), and phosphate buffer (pH 7.4) at 37 °C. The profile of Captopril release from γ-Fe_2O_3@SiO_2@captopril reveals that the maximum percentage drug release reaches about 79.93% at pH 1.2, 44.89% at pH 4.8, and 57.23% at pH 7.4.

CONCLUSION

In summary, we report the synthesis of Captopril-coated MNPs as a dual modal simultaneous for *T2* and *T2** negative MRI contrast agent and drug delivery system. γ-Fe_2O_3@ SiO_2@ captopril is an appropriate super-paramagnetic contrast agent which has the high relaxivity, high availability, high chemical stability, high magnetic moment and good dispersity. *In vitro* and *in vivo* MRI experiments confirmed the efficiency of γ-Fe_2O_3@SiO_2@captopril as contrast agent for MRI, it enhanced *T2*- and *T2**-weighted MRI sensitivity and consequently, excellent result of γ-Fe_2O_3@SiO_2@ captopril as contrast agent was observed at *in vivo* and *in vitro* MR images. The in vitro drug release, *in vivo* and *in vitro* MR imaging results was confirmed potential of γ-Fe_2O_3@ SiO_2@captopril as dual modal simultaneous for MRI contrast agent and drug delivery system. With these results, we can use MNPs-Captopril simultaneous for MRI contrast agent and drug delivery system.

ACKNOWLEDGMENTS

This work was supported by the Sistan and Baluchestan University.

REFERENCES

1. K. Swedberg, J. Kjekshus, CTS Group, *Am. J. Cardiol*., **62**, 60A – 66A (1988).
2. SOLVD Investigators, *New Engl. J. Med*., **325**, 293 – 302 (1991).
3. M. Ehlers, E. A. Fox, D. J. Strydom, and J. F. Riordan, *Proc. Natl. Acad. Sci. USA*, **86**, 7741 – 7745 (1989).
4. J. Pourahmad, M.-J. Hosseini, S. Bakan, and M. Ghazi-Khansari, *Pest. Biochem. Physiol*., **99**, 105 – 110 (2011).
5. M. Prabhu, S. Palaian, A. Malhotra, et al., *Kathmandu Univ. Med. J. (KUMJ*), **3**, 296 – 304 (2004).
6. H. Kubinyi, J. Taylor, and C. Ramdsen, *Compr. Med. Chem*., **4**, 589 (1990).
7. H.-P. Li, J.-J. Zhang, L. Qin, and M.-D. Zhao, *Res. Chem. Intermed*., **39**, 621 – 629 (2013).
8. J. Zeng, P. Du, L. Liu, et al., *Mol. Pharm*., **12**, 4188 – 4199 (2015).
9. H.-Y. Park, M. J. Schadt, L. Wang, et al., *Langmuir*, **23**, 9050 – 9056 (2007).
10. Z. Luo, K. Cai, Y. Hu, et al., Adv. Mater., **24**, 431 – 435 (2012).
11. L. Wang, J. Bao, L. Wang, et al., *Eur. J. Chem*., **12**, 6341 – 6347 (2006).
12. H. Qiu, B. Cui, G. Li, et al., *J. Phys. Chem. C*, **118**, 14929 – 14937 (2014).
13. L. Zhang, W.-F. Dong, and H.-B. Sun, *Nanoscale*, **5**, 7664 – 7684 (2013).
14. X. Zhang, L. Clime, H. Roberge, et al., *J. Phys. Chem. C*, **115**, 1436 – 1443 (2010).
15. H. B. Na, I. C. Song, and T. Hyeon, *Adv. Mater.*, **21**, 2133 – 2148 (2009).
16. S. Shen, F. Kong, X. Guo, et al., *Nanoscale*, **5**, 8056 – 8066(2013).
17. S. Laurent, D. Forge, M. Port, et al., *Chem. Rev*., **108**, 2064 – 2110 (2008).
18. G. Wang, X. Zhang, A. Skallberg, et al., *Nanoscale*, **6**, 2953 – 2963 (2014).
19. E. Terreno and S. Aime, *Front. Pharmacol*., **6**, 290 (2015).
20. B. H. McDonagh, G. Singh, S. Hak, et al., *Small*, **12**, 301 – 306 (2016).
21. Z. Bao, J. A. Rogers, and H. E. Katz, *J. Mater. Chem*. **9**, 1895 – 1904 (1999).
22. B. Z. Tang, Y. Geng, J. W. Y. Lam, et al., *Chem. Mater.*, **11**, 1581 – 1589 (1999).
23. K. M. Ho and P. Li, *Langmuir*, **24**, 1801 – 1807 (2008).
24. S. Sobhani,, Z. M. Falatooni, and M. Honarmand, *RSC Adv*., **4**, 15797 – 15806 (2014).
25. K. Azizi and A. Heydari, *RSC Adv*., **4**, 8812 – 8816 (2014).
26. Y. Zhang, M. Yang, N. G. Portney, et al., *Biomed. Microdev*., **10**, 321 – 328 (2008).
27. M. Khalkhali, S. Sadighian, K. Rostamizadeh, et al., *Nanomed. J*., **2**, 223 – 230 (2015).
28. N. Arsalani, H. Fattahi, and M. Nazarpoor, *Express Polym. Lett*., **4**, 329 – 338 (2010).
29. N. Lee and T. Hyeon, *Chem. Soc. Rev*., **41**, 2575 – 2589 (2012).
30. N. Sattarahmady, T. Zare, A. Mehdizadeh, et al., *Coll. Surf. B: Biointerf*aces, **129**, 15 – 20(2015).
31. T. He, P. D. Gatehouse, G. C. Smith, *Magn. Reson. Med*., **60**, 1082 – 1089 (2008).
32. T. He, P. D. Gatehouse, P. Kirk, et al., *Magn. Reson. Med*., **60**, 350 – 356 (2008).
33. X. Yang, J. J. Grailer, I. J. Rowland, et. al., *ACS Nano*, **4**, 6805 – 6817 (2010).
34. Y. W. Jun, J. H. Lee, and J. Cheon, *Angew. Chem. Intern. Ed.*, **47**, 5122 – 5135 (2008).
35. S. Sitthichai, C. Pilapong, T. Thongtem, and S. Thongtem, *App. Surf. Sci*., **356**, 972 – 977 92015).
36. S. Tong, S. Hou, Z. Zheng, et al., *Nano Lett*., **10**, 4607 – 4613 (2010).
37. R. Van Roosbroeck, W. Van Roy, T. Stakenborg, et al., *ACS Nano*, **8**, 2269 – 2278 (2014).
38. G. Fu, L. Zhu, K. Yang, et al., *ACS Appl. Mater. Interfaces*, **8**, 5137 – 5147 (2016).